## CONFERENCE PRE-PRINT

# EXPERIMENTAL AND NUMERICAL STUDY OF BROAD WAVENUMBER TURBULENCE AND TRANSPORT IN ION INTERNAL TRANSPORT BARRIER PLASMAS ON EAST

P. J. SUN, X. F. HAN, H. Q. LIU, Y. D. Li, G. S. LI, Y. F. WANG, S. X. WANG, T. ZHANG, H. L. ZHAO, Y. O.

Chu, H. LIAN, Y. F. JIN, L. Q. Xu, Q. ZANG, G. S. XU, J. P. Qian, Y. T. SONG AND THE EAST TEAM Institute of plasma physics, Chinese Academy of Sciences

Hefei, China

Email: sunpj@ipp.ac.cn

Y. REN Princeton Plasma Physics Laboratory Princeton, United States

Y. Xiao, S. Miao Zhejiang University Hangzhou, China

#### Abstract

In this work, we investigate microturbulence behavior spanning from ion to electron scales in the core plasma during internal transport barrier (ITB) formation in the EAST tokamak, employing a combined experimental and numerical simulation approach. Ion-scale turbulence ( $k < 5 \text{ cm}^{-1}$ ) was monitored via O-mode microwave reflectometry, while electron-scale turbulence ( $k = 10, 20 \text{ cm}^{-1}$ ) was detected using a CO<sub>2</sub> laser collective scattering diagnostic. During the ion ITB phase, obvious turbulence is observed at both ion and electron scales. Nonlinear gyrokinetic simulations using TGLF reveal that both ion-scale ITG turbulence and electron-scale ETG turbulence remain unstable. Quasilinear TGLF analysis further demonstrates that ion-scale turbulence drives both ion and electron heat transport, along with significant particle transport capacity. Notably, ion heat transport is substantially stronger than electron heat transport. Subsequent ion temperature gradient scans show that these transport fluxes increase with rising a/L<sub>Ti</sub>. In contrast, electron-scale ETG turbulence exhibits limited electron heat transport drive capability and negligible contribution to ion heat, particle, and momentum transport. Therefore, further suppression of ion-channel transport is essential for effectively enhancing ion temperature in EAST plasmas.

# 1. INTRODUCTION

The pursuit of controlled thermonuclear fusion as a sustainable energy source has driven extensive research on magnetically confined plasmas in tokamak devices. A critical challenge in this endeavour lies in understanding and controlling turbulent transport processes that limit plasma confinement and performance [1-2]. Internal transport barriers (ITBs) have emerged as a promising regime for improved confinement, characterized by locally steepened pressure gradients and suppressed turbulent transport in the plasma core [3]. Particularly, ion ITBs offer the potential for enhanced ion temperature profiles, which are crucial for achieving reactor-relevant conditions.

On the Experimental Advanced Superconducting Tokamak (EAST), the formation and sustainment of ion ITBs have been demonstrated under various operating scenarios [4]. However, the underlying microturbulence dynamics across different spatial scales during ITB formation remain incompletely understood. While large-scale turbulence suppression is often observed in ITB regimes, the behavior of broadband turbulence spanning from ion to electron scales requires detailed investigation. Ion-scale turbulence, primarily driven by ion temperature gradient (ITG) modes with normalized wavenumbers  $k\rho_i < 1$ , has long been recognized as a dominant contributor to anomalous transport in tokamak plasmas [5]. More recently, attention has turned to electron-scale turbulence, particularly electron temperature gradient (ETG) modes at higher wavenumbers  $k\rho_i > 1$ , which may contribute to residual electron heat transport even in improved confinement regimes [6-7].

Understanding the interplay between these different scale turbulences and their respective roles in transport is essential for optimizing confinement strategies. Previous studies on various devices have reported complex multiscale behaviour during ITB formation, with different scale turbulences exhibiting varying degrees of

suppression. The development of advanced diagnostics, including O-mode microwave reflectometry for ion-scale measurements and CO2laser collective scattering for electron-scale detection, now enables comprehensive characterization of broadband turbulence dynamics.

Complementary to experimental approaches, gyrofluid simulations using codes like TGLF (Trapped Gyro-Landau Fluid) provide powerful tools for interpreting experimental observations and elucidating the underlying physics mechanisms. The quasilinear capabilities of TGLF are particularly valuable for assessing the relative contributions of different instability types to various transport channels. However, validating these models against experimental data across multiple scales remains an ongoing challenge.

In this work, we present a combined experimental and numerical investigation of broadband turbulence and transport during ion ITB formation in EAST plasmas. Our study addresses several key questions: To what extent are ion-scale and electron-scale turbulences suppressed during ITB formation? What are the relative roles of ITG and ETG turbulences in driving heat, particle, and momentum transport? How do this transport channels respond to variations in key plasma parameters, particularly the ion temperature gradient?

The remainder of this paper is organized as follows: Section 2 describes the experimental setup, diagnostic systems, and numerical methods. Section 3 presents the experimental observations of broadband turbulence during ITB formation. Section 4 details the TGLF simulation results and quasilinear analysis of transport mechanisms. Section 5 summarizes the main conclusions and outlines future research directions.

## 2. EXPERIMENTAL SETUP, DIAGNOSTIC SYSTEMS, AND NUMERICAL METHODS

The experimental findings reported in this work were obtained on the EAST (Experimental Advanced Superconducting Tokamak) device. Subsequent numerical simulations were performed using experimental equilibrium profiles reconstructed via kinetic EFIT. EAST is a fully superconducting tokamak equipped with both toroidal and poloidal field magnets. Its main parameters include a major radius  $R \approx 1.85$  m, a minor radius \*a\*  $\approx 0.45$  m, a plasma current  $Ip \le 1$  MA, and an elongation  $\kappa$  varying between 1.2 and 2. The device supports operation in multiple magnetic configurations, including Lower Single Null (LSN), Upper Single Null (USN), Double Null (DN) divertors, as well as circular configurations.

A comprehensive set of diagnostics has been implemented on EAST for turbulence characterization. In this study, ion-scale density fluctuations were measured using an O-mode microwave reflectometer (REFL-fluc), operating at a fixed frequency of 52.6 GHz. This frequency corresponds to a cut-off density of approximately  $3.4 \times 10^{19}$  m<sup>-3</sup>, positioning the measurement near the normalized radial coordinate  $\rho \approx 0.3$  for the analyzed discharges. The maximum detectable wavenumber, kmax, is estimated to be about 5 cm<sup>-1</sup>, reflecting the diagnostic's sensitivity to ion-scale turbulence. Meanwhile, electron-scale turbulence was monitored using a CO<sub>2</sub> laser collective scattering system.

For numerical analysis of microturbulence, the Trapped Gyro-Landau Fluid (TGLF) model is employed. TGLF enables the computation of linear growth rates and real frequencies of dominant and subdominant modes, along with nonlinear turbulent transport fluxes of energy, particles, and momentum. A notable improvement of TGLF over its predecessor, the GLF23 model, lies in its enhanced accuracy in linear eigenmode calculations, as verified through extensive gyrokinetic benchmarks. The TGLF model computes eigenmode wavefunctions along magnetic field lines via an expansion in Hermite polynomials. Using a typical setup of 4 Hermite basis functions for three species (electrons, main ions, and impurities), the resulting equation system forms a matrix of dimension 180. Although larger than the matrix in GLF23, it remains computationally tractable for integrated modeling applications.

## 3. EXPERIMENTAL OBSERVATIONS OF BROADBAND TURBULENCE DURING ITB FORMATION

## 3.1. Overview of the discharge

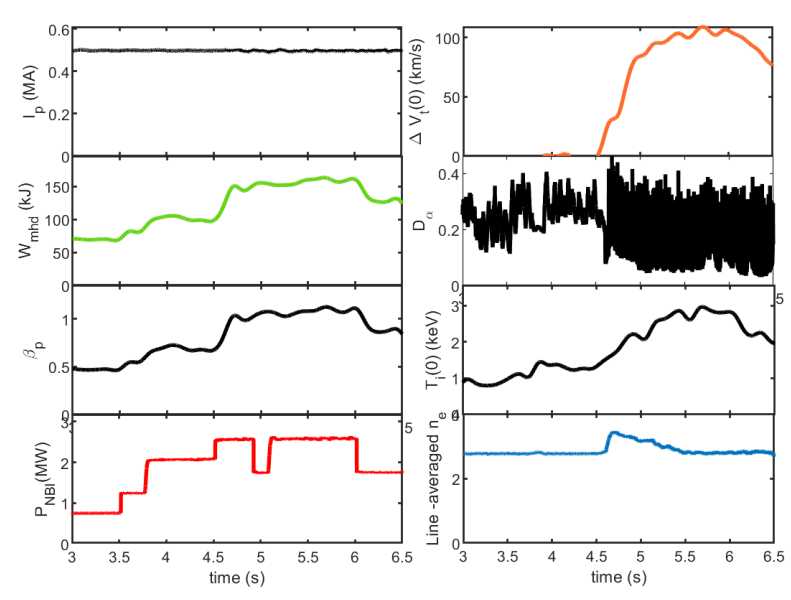


FIG. 1. An overview of discharge #103519 during t = 3 - 6.5 s. From top to bottom and left to right, the panels show: plasma current, stored energy, poloidal beta, NBI power, change in toroidal rotation velocity relative to t = 2.5s, D-alpha signal, central ion temperature, and line-averaged electron density.

Figure 1 presents an overview of plasma discharge #103519, which has been selected for in-depth analysis. The discharge features a deuterium plasma, and the observation of broadband turbulence is made during the L-mode and internal transport barrier (ITB) phases within the time window of t = 3-6.5 s. The plasma current was maintained at 500 kA, while the plasma stored energy increased from 70 kJ to 162 kJ. Neutral Beam Injection (NBI) served as the sole auxiliary heating method for this discharge, with power levels ramping up from approximately 0.8 MW to 2.6 MW. Starting at 4.5 s, the plasma transitions into an H-mode phase, as clearly indicated by a significant rise in the toroidal rotation velocity. Concurrently, the D-alpha signal exhibits characteristic edge-localized modes (ELMs), and the central ion temperature shows a marked increase. The lineaveraged electron density rises abruptly at the L-H transition but subsequently decays back to a level typical of L-mode. The peak central ion temperature is observed at t = 5.7 s. The following experimental and simulation analyses will focus specifically on this time point.

## 3.2. Observation of (ion, electron)-scale broadband turbulence

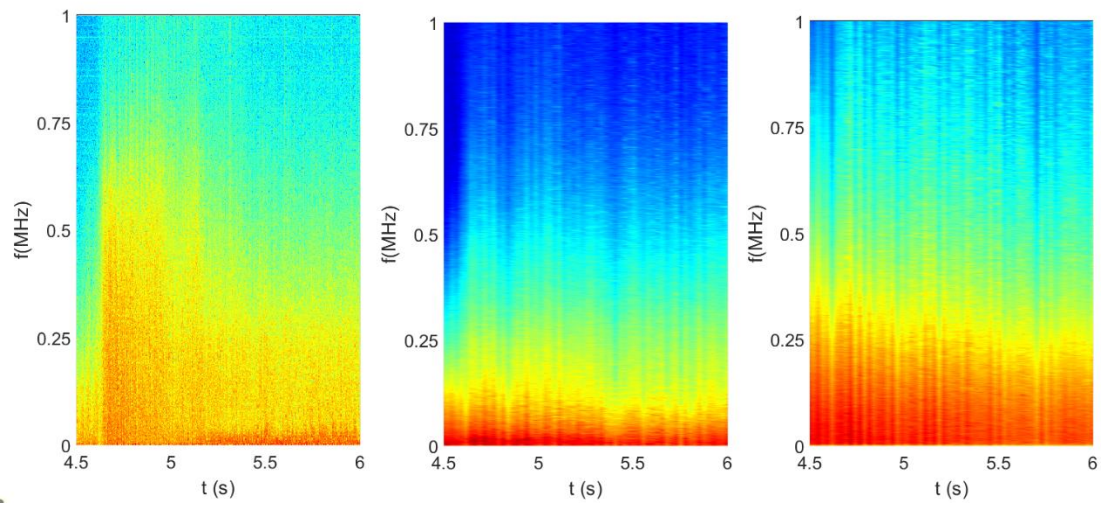


FIG. 2. From left to right: ion-scale turbulence (k < 5 cm<sup>-1</sup>) monitored by the O-mode microwave reflectometer, and electron-scale turbulence (k = 10, 20 cm<sup>-1</sup>) monitored by the  $CO_2$  laser coherent scattering system

To further investigate turbulence under NBI heating, we now present the ion-scale turbulence monitored by the O-mode microwave reflectometer and the electron-scale turbulence monitored by the  $CO_2$  laser coherent scattering system. Figure 2 displays the time-frequency spectrograms of density fluctuations for wavenumbers  $k < 5 \text{ cm}^{-1}$  and k = 10, 20 cm<sup>-1</sup>. Analysis of Fig. 2 reveals that, despite the improved confinement of the ITB H-mode plasma, both ion-scale and electron-scale turbulences remain significant. This observation necessitates further investigation to identify the specific types and dominant modes of the observed turbulence.

## 3.3. Plasma profiles, gradients and power balance analysis

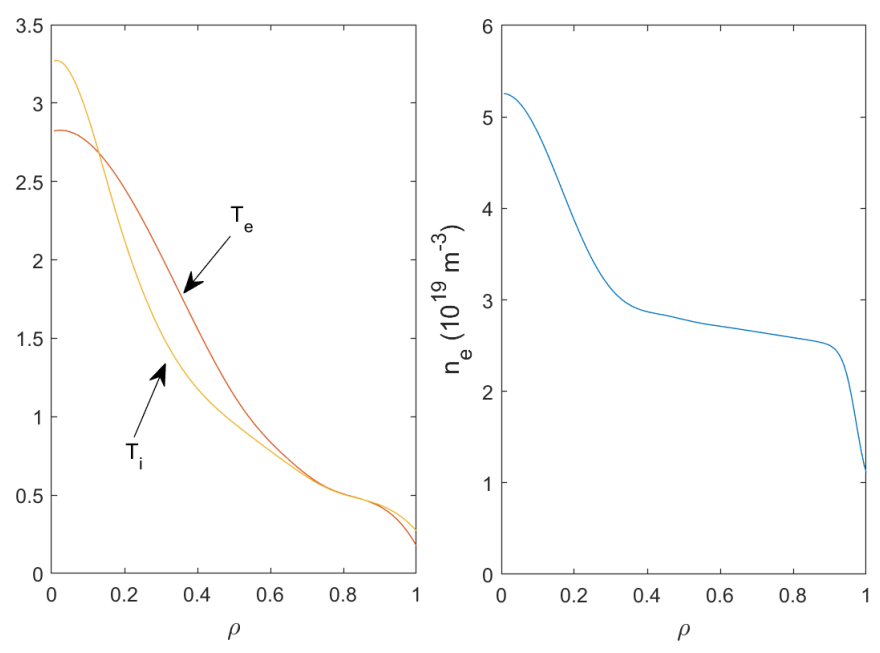


FIG. 3. From left to right: representative electron temperature, ion temperature, and electron density profiles during the ITB (Internal Transport Barrier) plasma phase.

Figure 3 displays the electron temperature, ion temperature, and electron density profiles. Several key features can be clearly observed: in the plasma core, the ion temperature exceeds the electron temperature. Additionally, both the ion temperature and electron density profiles exhibit clear internal transport barriers (ITBs). The foot of the ITB is located at approximately  $\rho = 0.35$ . Here,  $\rho$  represents the normalized toroidal magnetic flux. Experimentally, the ion-scale turbulence is monitored around  $\rho = 0.3$ , a region that approximately coincides with the area of strongest gradient within the steep ITB. The power deposition profiles for ions and electrons serve as critical heating sources in the plasma, and are important factors influencing the electron temperature Te, ion temperature Ti, and the observed saturated turbulence levels. The NUBEAM code being a Monte Carlo fast-ion module was employed to compute the power deposition and driven current from neutral beam injection (NBI). Neoclassical transport properties for a multi-species, axisymmetric plasma with arbitrary aspect ratio, geometry, and collisionality were evaluated using the NCLASS module. By integrating the NUBEAM and NCLASS modules within the TRANSP framework, we obtained the ion and electron power deposition profiles resulting from both NBI and Ohmic heating, as shown in Fig. 4. The underlying plasma equilibrium is based on kinetic EFIT reconstructions, constrained by Faraday rotation angle measurements from the POINT diagnostic and experimental plasma profiles. This same kinetic EFIT equilibrium will also be used in subsequent simulations. Figure 4 presents the plasma current density and power deposition profiles, which are further broken down into their respective components: total current and total power, Ohmic current and power, as well as NBI-driven current and bootstrap current profiles. Analysis of the current profile reveals that the plasma current is predominantly sustained by the Ohmic component, with the bootstrap current also making a notable contribution in the core region. In terms of power deposition, neutral beam injection primarily heats ions within the normalized radius  $\rho < 0.6$ . Both NBI and Ohmic heating also contribute to electron heating; however, the core region ( $\rho < 0.6$ ) 0.6) remains predominantly electron-heated. This heating balance explains the observed central ion temperature exceeding the electron temperature in the plasma core.

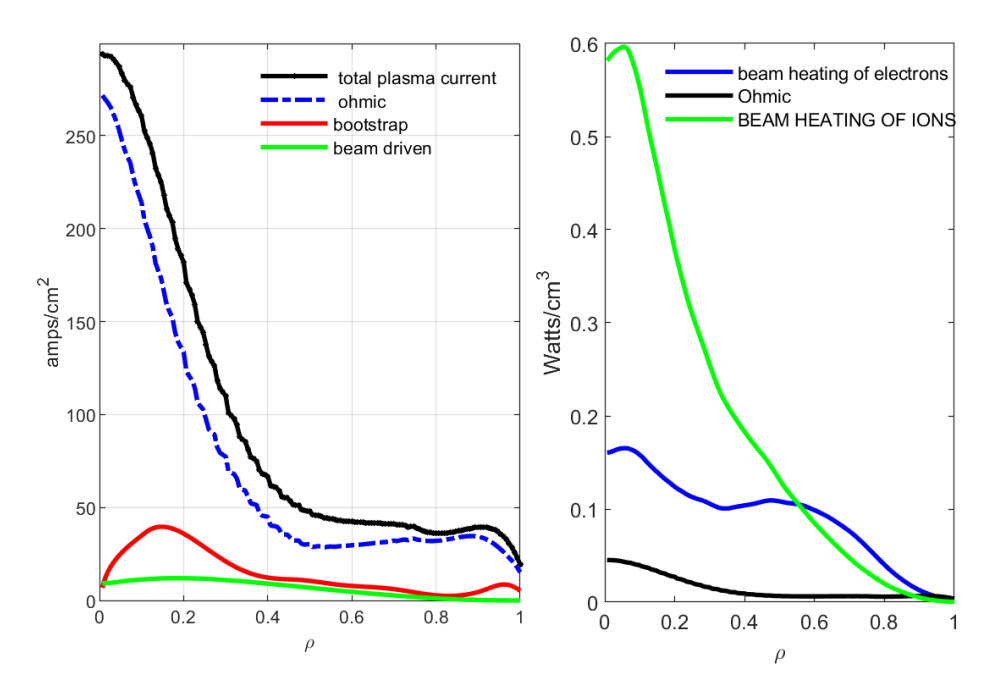


FIG. 4. From left to right: current density profiles (including total, Ohmic, bootstrap, and NBI-driven currents) and power deposition profiles (including electron and ion deposition from NBI, as well as Ohmic power).

## 4. TGLF SIMULATION RESULTS AND QUASILINEAR ANALYSIS OF TRANSPORT MECHANISMS

Although experimental determination of microturbulence thresholds remains challenging, these thresholds play a critical role in governing turbulent saturation levels and transport magnitudes. We therefore begin by performing a stability analysis using established analytical and empirical models to compute linear thresholds for microinstabilities. The critical gradients are evaluated with the Profiles-gen code, which incorporates the IFS/PPPL modelfor the ITG critical gradient R/LTi, the Jenko model for the ETG critical gradient R/LTe, and the Peeters model for the threshold of electron temperature gradient-driven TEM. Figure 5 compares the experimentally normalized gradient scale lengths R0/LTi and R0/LTe (solid red lines) with the corresponding instability thresholds (dashed blue and black lines) for ITG, TEM, and ETG modes.

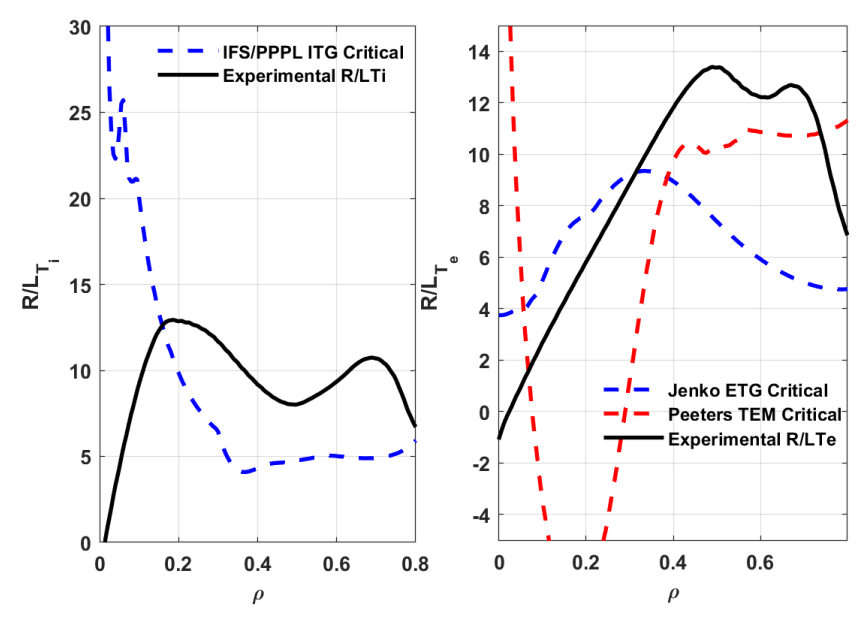


FIG. 5. Comparison of the measured gradient scale lengths R0/LTe and R0/LTi (solid red line) against the critical thresholds for various micro-instabilities: ITG (dashed blue line), TEM (dashed black line), and ETG (dashed green line).

As shown in the left panel of Figure 5, the critical threshold for the ITG mode lies below the experimentally measured R0/LTi in the region  $\rho$ <0.2, whereas the mode becomes linearly unstable for  $\rho$ >0.2. The TEM mode is linearly unstable across the interval  $0.1<\rho$ <0.7, while the ETG mode remains linearly stable for  $\rho$ <0.3 but transitions to linear instability beyond  $\rho$ >0.35 relative to its critical gradient. Consequently, at the radial location  $\rho$ <0.3, where ion-scale turbulence is experimentally observed, both ITG and TEM modes are likely excited, whereas the ETG mode lies near marginal stability.

Although the analytic and empirical models employed above allow a preliminary assessment of ITG, TEM, and ETG stability near the monitored turbulence location ( $\rho$ ~0.3), they cannot identify the dominant instability type, quantify growth rates, or predict transport levels. To address these limitations, we turn to quasi-linear modeling using the TGLF code. Notably, TGLF was developed to improve the accuracy of linear eigenmode calculations compared to the earlier GLF23 model and has demonstrated better agreement with gyrokinetic benchmarks in eigenvalue computations. The model solves for linear eigenmodes along magnetic field lines via an expansion in Hermite polynomials. With 4 Hermite basis functions and three species (electrons, ions, and impurities), the resulting TGLF equation system forms a matrix of dimension  $15 \times 4 \times 3 = 180$ . Although substantially larger than the matrix in GLF23, it remains computationally tractable for integrated modeling applications.

To match experimental turbulent fluxes quantitatively, quasi-linear models typically incorporate physics-constrained saturation rules. This approach circumvents the prohibitive computational cost of self-consistently simulating turbulent self-organization within a quasi-linear framework. After nearly two decades of TGLF development, multiple saturation rule options have been established. For EAST experimental analysis, SAT0 and SAT1 generally yield reliable results, whereas SAT2 often encounters convergence issues.

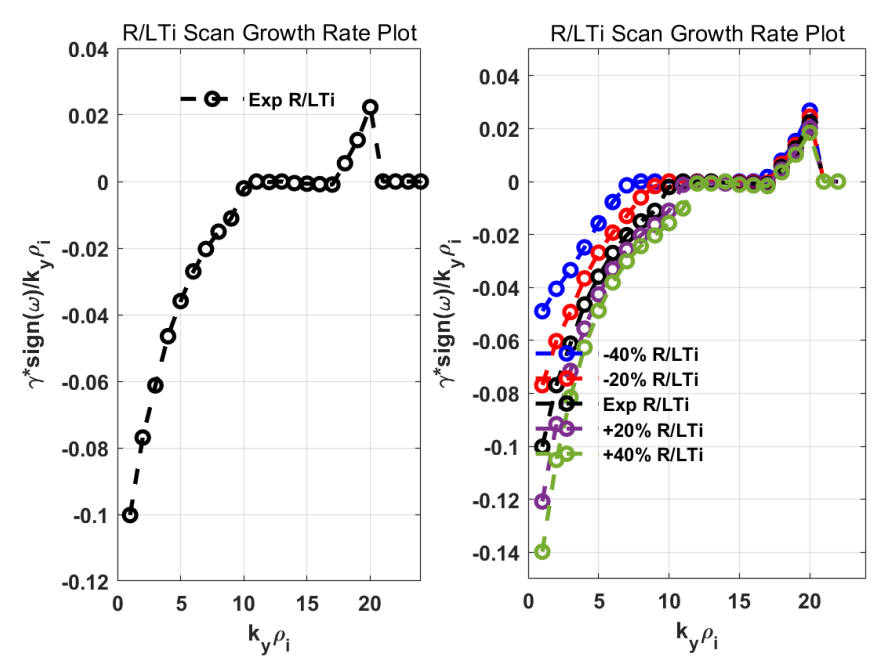


FIG. 6. From left to right: Linear growth rate multiplied by the mode propagation direction sign for ion-scale and electron-scale micro-instabilities, respectively. Parameter scans of R0/LTi dependencies.

The left panel of Figure 6 displays the linear growth rate multiplied by the mode propagation direction sign for ion-scale and electron-scale micro-instabilities, respectively. It can be clearly observed that modes with kypi <10 propagate in the ion diamagnetic drift direction, while modes near kypi≈20 propagate in the electron diamagnetic drift direction. This is consistent with the experimentally observed ion-scale and electron-scale turbulence.

To further investigate the dependence of ion-scale and electron-scale instability modes on R0/LTi, we performed a scan over this parameter. The results, shown in the right panel of Figure 6, indicate that the normalized growth

rate of ion-scale micro-instabilities increases with R0/LTi, whereas electron-scale micro-instabilities exhibit an opposite trend.

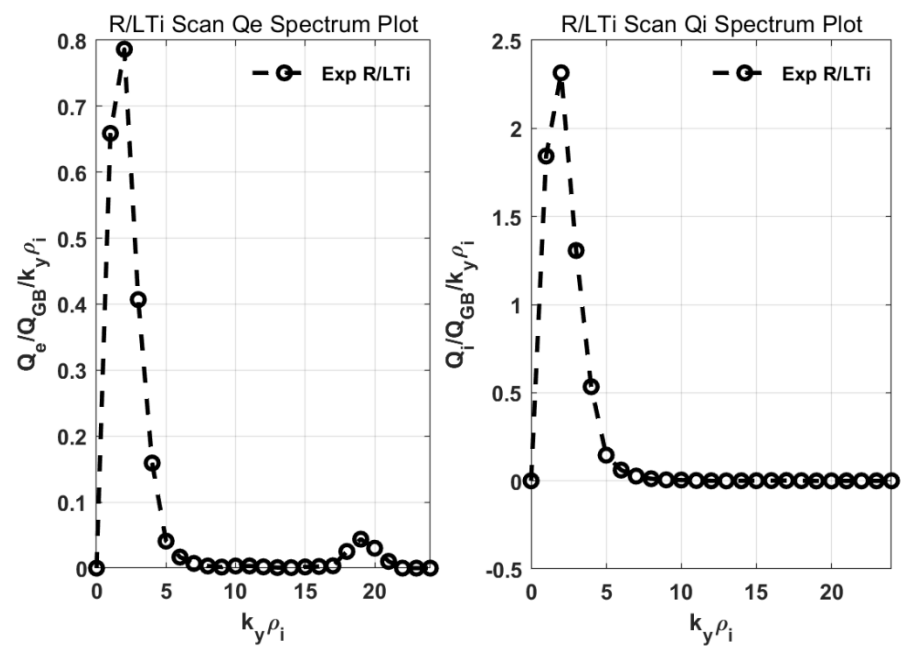


FIG. 7. From left to right: Normalized electron heat flux, ion heat flux

Having identified the ion-scale and electron-scale instabilities, we now proceed to examine their respective transport capabilities. We employ quasi-linear TGLF simulations to calculate the normalized electron and ion heat fluxes. The left panel of Figure 7 shows that the normalized electron heat flux primarily originates from modes with kypi<5, with a secondary contribution from modes near kypi~20. The right panel indicates that the normalized ion heat flux is also dominated by modes in the kypi<5 range, while modes around kypi~20 contribute negligibly to ion heat transport. Furthermore, the normalized ion heat flux is significantly larger than its electron counterpart, indicating that the ion-scale turbulence (kypi<5) predominantly drives ion thermal transport.

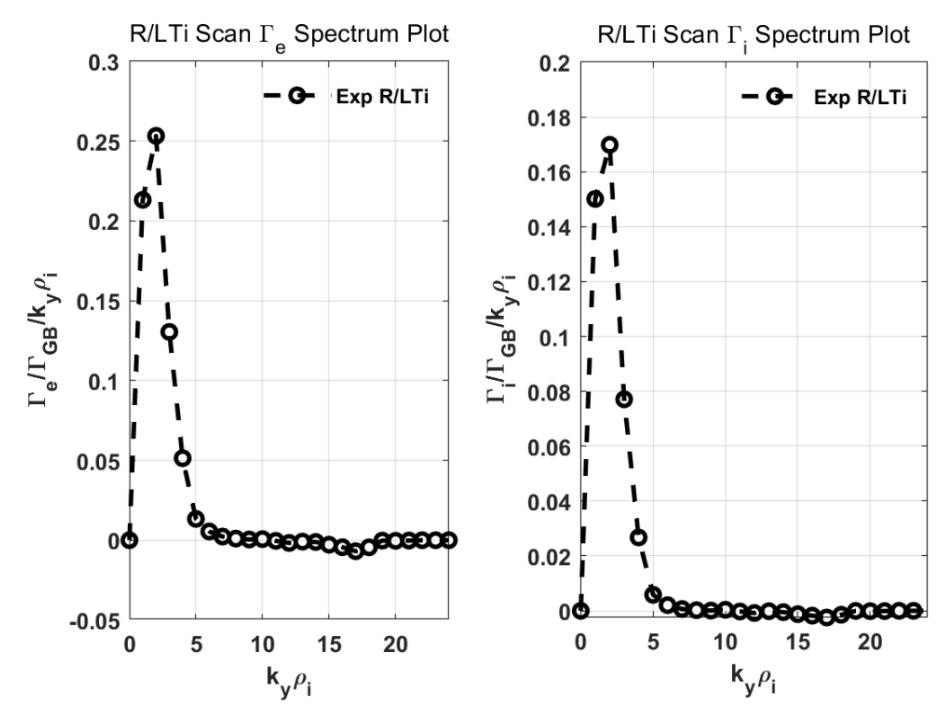


Fig.8: From left to right: Normalized electron and ion particle flux

Figure 8 presents the normalized electron and ion particle fluxes from TGLF simulations. It can be observed that both the normalized electron and ion particle fluxes are primarily driven by ion-scale turbulence with kypi<5. The

normalized electron particle flux is slightly higher than its ion counterpart, though their overall magnitudes remain comparable.

Therefore, the TGLF linear simulations not only corroborate the experimentally observed distinct electron-scale and ion-scale turbulence, but also further demonstrate that the ion-scale turbulence ( $ky\rho i < 5$ ) can drive significant ion and electron heat transport, as well as moderate particle transport for both species. Consequently, targeted suppression of turbulent transport is essential for further enhancing the ion temperature.

## 5. SUMMARY

In summary, integrated experimental and simulation analysis of EAST tokamak discharges, this work investigates multiscale microturbulence behavior during the formation of an ion internal transport barrier (ITB). Ion-scale (k < 5 cm<sup>-1</sup>) and electron-scale (k = 10, 20 cm<sup>-1</sup>) turbulence were monitored simultaneously using O-mode microwave reflectometry and CO<sub>2</sub> laser collective scattering, respectively. During the ITB phase, pronounced turbulence is observed across both scales. Nonlinear and quasilinear analyses with the TGLF model confirm that ion-scale ITG and electron-scale ETG instabilities remain active. The simulations further reveal that ion-scale turbulence drives significant ion and electron heat transport, with ion heat transport being substantially stronger, as well as notable particle transport. Transport fluxes increase with the ion temperature gradient a/LTi, whereas electron-scale ETG turbulence contributes only weakly to electron heat transport and negligibly to ion and particle transport. These findings highlight that targeted suppression of ion-scale turbulent transport is essential for further enhancing core ion temperature in EAST.

#### **ACKNOWLEDGEMENTS**

This work was supported by the Fusion Energy R&D Program of China under Grant Nos. 2024YFE03190002, 2024YFE03190004, the National Natural Science Foundation of China under Grant Nos. 12275316, 12475233.

## REFERENCES

- [1] B. Coppi et al., Phys. Fluids 10, 582 (1967).
- [2] B. B. Kadomitsev and O. P. Pogutse, Reviews of Plasma Physiscs, Turbulence in Toroidal Systems (New York: Consultants Bureau) (1970).
- [3] K. Ida, et al. Plasma Phys. Control. Fusion, 60 (2018)
- [4] X. Gao, et al. Nucl. Fusion, 57 (2017)
- [5] P. J. Sun, et al., Nucl. Fusion 65, 086014 (2025)
- [6] Y. Ren et al., Rev. Mod. Plasma Phys. 8, 5 (2024).
- [7] Y. Ren et al., Nucl. Fusion 57, 072002 (2017).